RSC Advances

Electron induced chemistry for Acetaldehyde

Journal:	*RSC Advances*
Manuscript ID:	RA-ART-07-2015-012866
Article Type:	Paper
Date Submitted by the Author:	02-Jul-2015

Complete List of Authors:	VINODKUMAR, MINAXI; V.P & R.P.T.P. SCIENCE COLLEGE, ELECTRONICS; P.G. DEPARTMENT OF PHYSICS, SARDAR PATEL UNIVERSITY, PHYSICS Limbachiya, Chetan; The M. S. University Baroda, Vadodara - 390001, Department of applied Physics DESAI, HARDIK; DEPARTMENT OF PHYSICS, SARDAR PATEL UNIVERSITY, VALLABH VIDYANAGAR, PHYSICS VINODKUMAR, P.C.; DEPARTMENT OF PHYSICS, SARDAR PATEL UNIVERSITY, VALLABH VIDYANAGAR, PHYSICS

Electron induced chemistry for Acetaldehyde

Minaxi Vinodkumar*[a], Chetan Limbachiya[b], Hardik Desai,[c] and P C Vinodkumar[c]

Received Xth XXXXXXXXXX 20XX, Accepted Xth XXXXXXXXX 20XX
First published on the web Xth XXXXXXXXXX 200X
DOI: 10.1039/b000000x

A detailed theoretical study is carried out for electron interactions with acetaldehyde (CH_3CHO) with impact energies ranging from 0.01 eV to 5000 eV. Owing to the wide energy range we have been able to investigate variety of processes and report data on Dissociative Electron Attachment (DEA) through resonances, vertical electronic excitation energies, differential, momentum transfer, ionization and total cross sections (TCS) as well as scattering rate coefficients. In order to compute TCS we have employed ab initio R-matrix method (0.01 eV to $\sim$ 20 eV) and the spherical complex optical potential (SCOP) method ($\sim$ 20 eV to 5000 eV). The R-matrix calculations are performed using close coupling method employing static exchange plus polarization model. We have employed different target models and basis sets to study their effect on the target parameters as well as total cross sections. We observed two strong resonances, one at 1.33 eV which corresponds to 2A" symmetry with a width of 0.1726 eV which is in agreement with 1.30 predicted earlier experimentally by van Veen et. al.[7] and other resonance at 10.03 eV of 2A' symmetry with 0.0688 eV width which is close to 10.00 eV reported experimentally by Szymanska[18]. The first peak corresponds to capture of an electron in to the lowest vacant $\pi*$ orbital of the carbonyl group while the second corresponds to $\sigma*$ core excited shape resonance which is responsible for O^- fragment. We observed many fragments of CH_3CHO in our eigenphase sum study which are in accordance with the earlier reported data[7,10,16,18]. The scattering rate coefficients and theoretical TCS data beyond 30 eV are reported for the first time. Further, no experimental data for TCS is available beyond 400 eV to the best of our knowledge. We have compared all our results with available data in the literature and found overall good agreement. Due to dearth of TCS data for acetaldehyde, we have also compared the TCS of acetaldehyde with its analogue targets such as formic acid, formaldehyde, formamide and ethylene oxide and drawn conclusions.

1 Introduction

Acetaldehyde, the simplest aldehyde, is one of the first identified organic molecules in the interstellar space[1–3]. The presence of acetaldehyde in both giant molecular clouds[4] and dark clouds[5] has geared up interests of many astrochemists to focus on this molecule. The observation of larger and more complex molecules will be a major objective of the new ALMA telescope array including the search for prebiotic molecules. Multiple proton transfer in H-bonded species is indeed one of the fundamental molecular mechanisms in biology, as it governs oxidation-reduction steps in many reactions. Indeed various gas-phase synthetic routes have been suggested[6] for the formation of different molecules from these simple precursors by electron interaction. Hence, the search for prebiotic molecules beyond solar system, especially in the interstellar medium is one of the most exciting topics for astrochemistry since, if found, their presence would suggest that the 'ingredients' of life are common to star and planet formation and hence life may have the opportunity to develop in many 'solar like systems' and is not restricted to the special conditions on Earth. Thus to study the origin of life, low and intermediate energy electron collision studies on these interstellar molecules are of great significance.

Reviewing the previous studies of electron impact on acetaldehyde we find experiments of van Veen and coworkers [7] and Jordan and Burrow[8] using the transmitted electron current which is sensitive to the presence of narrow elastic resonances. The expected C=O $\pi*$ shape resonance was observed at 1.19 eV[8] and at 1.3 eV[9] respectively. In an electron energy-loss experiment, Dressler and Allan[10] observed electronic Feshbach resonances between 6 and 7 eV. Measured cross sections for vibrational excitation by electron impact have shown both the $\pi*$ shape resonance[9,10] at about 1.2 eV, and a broad peak at 6.8 eV, assigned to one or more $\sigma*$ resonances[10]. Other measurements have determined thresholds and, in some cases, relative cross sections for electronic excitation[7,10–15], while still others have examined dissociative electron attachment[10,16–18]. Burean and Swiderek[19] have studied the chemistry induced in condensed acetaldehyde by low-energy electron impact. However scattering studies

[a] *V P & R P T P Science College, Vallabh Vidyanagar - 388 120, India; E-mail: minaxivinod@yahoo.co.in*
[b] *Department of applied Physics, The M. S. University Baroda, Vadodara - 390001, India.; E-mail:chetanlimbachiya2@yahoo.com*
[c] *Department of Physics, Sardar Patel University, Vallabh Vidyanagar - 388120, India; E-mail:hardikdesai.phy@gmail.com; E-mail:p.c.vinodkumar@gmail.com*

on electron impact on total cross sections of acetaldehyde is scanty. Electron impact collision cross sections are reported by only two groups. Recently Gauf *et. al.*[20] reported both experimental and theoretical results of electron collision cross sections with acetaldehyde. They reported cross section measurements from 0 to 50 eV and calculations are reported till 30 eV. Szmytkowski *et. al.*[21] reported electron impact total cross sections for acetaldehyde from 0.7 to 400 eV using linear electron transmission method. Thus literature survey makes it very clear that data on electron scattering total cross sections with acetaldehyde is sparse. Beyond 30 eV there is no theoretical TCS reported to the best of our knowledge.

Survey on electron impact ionization cross section literature reveals that there are more measurements[22–26] than calculations[23,27]. Harrison et. al.[25], Otvos & Stevenson[26] and Beran and Kevan[24] reported measured Q_{ion} for acetaldehyde at 75 eV and 70 eV respectively. Many experimentalist measure partial/total ionization cross section at 70 eV or 75 eV since this energy is commonly used in Mass Spectrometry devices. Experimentally, Vacher et. al.[23] used mass spectrometry technique to measure the Q_{ion} for acetaldehyde, which was obtained as a sum of partial cross sections for the ions. Recently, Bull and Harland[22] reported measured Q_{ion} for acetaldehyde. Theoretical data on Q_{ion} was recently reported by Gupta and Antony[27] using Complex scattering ionization cross section (CSP-ic) method and earlier by Vacher et. al.[23] using BEB method.

Aim of the present study is two fold, one to detect the resonances or transient negative ion formation which are very important at low energies as their study leads to proper understanding of the fragmentation and dissociation of the target leading to better comprehension of the structure of the target and second to fill the void of the total cross sectional data as earlier work is fragmentary. Further, due to scanty TCS data for acetaldehyde we have compared our TCS data with the analogues molecules such as formic acid (structurally similar)[28] , formaldehyde[28] , formamide[29] and ethylene oxide[30](isoelectronic) to study the functional group dependence on total cross sections.

2 THEORETICAL METHODOLOGY

We report here TCS over a wide energy range since a single theoretical formalism cannot be employed for diverse physical phenomena occurring at low and intermediate to high energy range. For the low impact energies (0.01 eV to about 20 eV) we employed the ab initio calculations using Quantemol − N[31] which utilizes UK molecular R-matrix code[32]. At low impact energies the TCS is a sum of total elastic and total electronic excitation (inelastic contribution) cross sections. The SCOP method is employed for calculating TCS beyond ionization threshold up to 5 keV[33]. Outline of these two formalisms are briefly given in the following subsections. Accuracy of low energy calculations is largely dependent on the target model employed. Hence before going to the theoretical methods we first furnish the details of target model employed for the present system.

2.1 TARGET MODEL

For precision of target properties as well as the scattering data, it is imperative to have an appropriate target model. For many-electron targets like CH_3CHO, the relative energy between the N-target electrons and the N+1 target plus scattering electron becomes important since neither the target nor the scattering wave functions have the energies close to the exact value for the given system. The major parameters involved in careful choice of the configurations are complete active space (CAS) and the valance configuration interaction (CI) representation of the target system[31]. It is obtained by carefully characterizing the low lying electronic states of the target and by generating a suitable set of orbitals. The molecular orbitals are generated by performing a self-consistent field (SCF) calculation of the ground state of the molecule ($X1A_1$). Since the SCF procedure is inadequate to provide a good representation of the target states, we improve the energies of these states by invoking the variational method of configuration interaction (CI) in which we take linear combination of configuration state functions (CSFs) of a particular overall symmetry. This lowers the energies and the correlation introduced provides a better description of the charge cloud and the energies. For all the states included here, we employ CI wave function to represent the target states.

For the optimised nuclear geometry of the target we employed second order Möller-Plesset perturbation theory in the 6-31G(d) basis set. The Hartree-Fock electronic configuration for the ground state of CH_3CHO at its equilibrium geometry in Cs symmetry is $1a'^2$, $2a'^2$, $3a'^2$, $4a'^2$, $5a'^2$, $6a'^2$, $7a'^2$, $8a'^2$, $1a''^2$, $9a'^2$, $2a''^2$ and $10a'$. Out of 24 electrons, 20 electrons are frozen in 1a', 2a', 3a', 4a', 5a', 6a', 7a', 8a', 9a', 1a" orbitals and 4 electrons are kept free to move in active space of 10a', 11a', 12a', 13a', 2a", 3a", 4a" molecular orbitals. All calculations of CH_3CHO are performed in Cs symmetry since the R-matrix code can only handle calculations in a subgroup of the highest accessible Abelian point group D2h. We have used cc-pVDZ, 6-31G and DZP basis sets in order to study the dependency of target properties and scattering cross sections on the basis set chosen.

The target wave functions are computed using the complete

active space configuration integration (CAS−CI) method. They are subsequently improved using a pseudo-natural orbital calculation. The Born correction for this polar molecule is employed to account for higher partial waves, $l > 4$. In the static-exchange-polarization (SEP) model, the ground state of the molecule is perturbed by single and double excitations of the electrons, thus leading to the inclusion of polarization effects. The SEP model augments the Static - exchange (SE) model by including polarization effects. Thus polarization effects are accounted by including closed channels in a CI expansion of the wave function of the entire scattering system. These electronic and angular momentum channels altogether generated 2637 configuration state functions (CSFs) and 365 channels in the calculation. The six lowest Cs electronic excited states (1A', 3A", 1A", 3A', 3A' and 1A') around the ionization threshold of the target using 6-31 G basis set and eight electronic excited states (1A', 3A", 1A", 3A', 3A', 1A',3A',1A') using cc-pVDZ are reported in Table 2. Thirty electronic excited target states employed all possible single and double excitations to virtual orbitals.

The Quantemol-N modules GAUSPROP and DENPROP [34] construct the transition density matrix from the target eigenvectors obtained from Configuration Integration (CI) expansion and generate the target properties. The multipole transition moments obtained are then used to solve the outer region coupled equations and the dipole polarizability α_0. These are computed using second-order perturbation theory and the property integrals are evaluated by GAUSPROP[34]. Our self-consistent field (SCF) model calculations yielded target parameters such as the ground state energy, the first electronic excitation energy, rotational constant and dipole moment which are listed in Table 1.

Table 1 Target properties obtained for the acetaldehyde molecule using 6-31G and cc-pVDZ basis sets

Target property (Unit)		Present		Other
		6-31G	cc-pVDZ	Th./Exp.
Ground State Energy (Hartree)		-152.86	-152.94	-153.69[35]
First Excitation Energy (eV)		4.88	5.21	4.49[47]
				4.38[35]
				4.3[36]
Rotational Constant (cm^{-1})	A	1.9123	1.9123	1.8877[37]
	B	0.3375	0.3375	0.3390[37]
	C	0.3029	0.3029	0.3035[37]
Dipole Moment (Debye)		3.24	2.87	2.75[38,39]
				2.69[37]
				2.6[41]

The self-consistent field calculations yielded the ground state energy of -152.86 Hartree using 6-31G and -152.94 Hartree using cc-pVDZ basis sets which are close to -153.69 Hartree reported earlier in literature[35]. We report first six electronic excitation states below ionization threshold of the target for acetaldehyde with the first electronic excitation energy obtained at 4.84 eV using 6-31G and at 5.21 eV using cc-pVDZ basis sets which are slightly higher compared to 4.38 eV, 4.49 eV and 4.3 eV reported earlier in[35], by Wiberg et. al.[47] and by Walsh[36] respectively. The present rotational constants of A = 1.9123 cm^{-1} , B = 0.3375 cm^{-1} and C = 0.3029 cm^{-1} are in good agreement with A = 1.8877 cm^{-1}, B = 0.3375 cm^{-1} and C = 0.3029 cm^{-1} respectively reported in CCCBDB[37]. The dipole moment obtained through present calculations are 3.24 D using 6-31G and 2.87 D using cc-pVDZ. The dipole moment obtained using cc-pVDZ is slightly higher compared to experimental value of 2.75 D reported by Paul and Cox[38] and in CRC handbook[39], 2.69 D reported in CCCBDB database [37] (originally reported by Nelson et. al.[40]) and 2.6 D reported earlier by Maria et. al.[41]. It can be easily seen that dipole moment is very sensitive to the basis set chosen and cc-pVDZ gives better value of dipole moment. Also inclusion of large diffused functions can improve upon the dipole moment but we cannot use diffuse functions for the target representation as this would violate the boundary condition that the target molecular orbitals should vanish on the surface of the R-matrix sphere[42]. Thus a satisfactory reproduction of the target properties is the cross check of proper target model employed for the present calculations.

Table 2 Vertical excitation energies for CH_3CHO below ionization threshold of target

State	Energy (eV)		
	6-31G	cc-pVDZ	Others
1A'	0.00	0.00	-
3A"	4.88	5.21	4.49[47]
1A"	5.40	5.75	5.73[47]
3A'	6.89	7.26	6.88[47]
	-	-	6.82[12,36]
	-	-	6.97[12,36]
	-	-	7.25[10]
3A'	10.37	9.71	9.51[12]
	-	-	9.5[36]
	-	-	9.4[7]
1A'	11.09	10.15	-
3A'	-	10.87	-
1A'	-	11.11	-

2.2 Low energy formalism (0.01 ∼ 15 eV)

Low energy electron collision calculations are performed using three most popular methodologies viz. the Kohn variational method[43,44], the Schwinger multichannel method

[45,46], and the R-matrix method[32]. Out of these three methods, R matrix is the most widely used method. The basic idea underlying the R-matrix method[32] is splitting of the configuration space into an inner region, which is a sphere of radius 'a' about the target center of mass, and an outer region. The boundary between these two regions is defined by R-matrix radius. This radius is chosen large enough so that, exchange and electron-electron correlation becomes negligible beyond this boundary. Thus in the external region, only known long-range forces are effective. In the inner region full electron-molecule problem is solved using Quantum Chemistry codes which consumes almost 90% of the total computational time. The inner region is usually chosen to have a radius of 10 au and the outer region is extended to about 100 au. The choice of this value depends on the stability of results obtained in the inner region and outer region calculations. We describe the scattering within the fixed-nuclei (FN) approximation that neglects any dynamics involving the nuclear motion (rotational as well as vibrational), whereas the bound electrons are taken to be in the ground electronic state of the target at its optimized nuclear geometry. This is an effect of the extent of electronic charge density distribution around the center of mass of the target. In the present study we have considered 13 au of inner R-matrix radius.

In the inner region the total wave function for the system is written as,

$$\Psi_k^{N+1} = A\sum_I \Psi_I^N(x_1,...,x_N)\sum_j \zeta_j(x_{N+1})a_{Ijk} + \sum_m \chi_m(x_1,...,x_{N+1})b_{mk} \quad (1)$$

where A is an antisymmetrization operator introduced so that the indistinguishable inner-region electrons satisfy the Pauli principle, x_N is the spatial and spin coordinate of the n^{th} target electron, ζ_j is a continuum orbital spin-coupled with the scattering electron with a partial wave expansion up to some maximum value of l, say l_{max}, a_{Ijk} and b_{mk} are variationally optimized coefficients. The summations in the first term runs over the thirty target states used in the close-coupled expansion. The second summation in equation (1) runs over configurations χ_m, which describe all N+1 electrons but vanish at r = a; thus these are described as L^2 configurations. They are included to relax the constraint of orthogonalization between scattering and target orbital. In our inner region calculations, polarization effects are considered using second sum in equation (1) using singly excited L^2 configurations of the Hartree-Fock (HF) ground state wave function. This is achieved by promoting one target electron into a virtual (unoccupied target) orbital and simultaneously also placing the scattering electron into a virtual orbital generating a two-particle one-hole (2p,1h) configuration. This model is usually denoted static exchange plus polarization (SEP) model.

The target and the continuum orbitals are represented by Gaussian Type Orbitals (GTOs) and the molecular integrals are generated by the appropriate Molecular Package. The R-matrix will provide the link between the inner region and outer region. For this purpose the inner region is propagated to the outer region until its solutions match with the asymptotic functions given by the Gailitis expansion[32]. Thus by generating the wave functions, using Eq. 1, their eigenvalues are determined. These coupled single centre equations describing the scattering in the outer region are integrated to identify the K - matrix elements. The K - matrix is a symmetric matrix whose dimensions are the number of channels. All the observable are basically deduced from it and further it is used to deduce T matrix using the relation:

$$T = \frac{2iK}{1-iK} \quad (2)$$

The T - matrices are in turn used to obtain various total cross sections. The K − matrix is diagonalized to obtain the eigenphase sum. The eigenphase sum is further used to obtain the position and width of the resonance by fitting them to the Breit Wigner profile[48] using the program RESON[49]. The module structure of target calculations for the Quantemol-N UK molecular R-matrix code for inner region and outer region calculations are discussed elaborately in our earlier publication[53] and hence not repeated here.

Differential and Momentum transfer cross sections (MTCS) are calculated using POLYDCS program[50]. Differential Cross section (DCS) study is very important as it provides large information about the interaction processes. Indeed, the evaluation of DCS is stringent test for any scattering theory as it is sensitive to effects which are averaged out in integral cross sections. The procedure to evaluate DCS for polyatomic molecule is discussed in our earlier publications[53,58] and hence not repeated here. The calculated dipole moment (2.87 D) and rotational constants (A=1.9123 cm^{-1}, B=0.3375 cm^{-1}, C=0.3029 cm^{-1}) for CH_3CHO are used in the calculation of elastic DCS (J=0 → J'=0) and rotationally inelastic (J=0 → J' = 1, 2, 3, 4 and 5) DCSs at different collision energies.

The MTCS is obtained by integrating the differential cross sections (DCS) with a weight factor (1-cosθ).

$$\sigma_m = 2\pi \int \frac{d\sigma}{d\Omega}(1-cos\theta)d\theta \quad (3)$$

2.3 Higher energy formalism (Threshold to 5 keV)

For scattering calculations above the ionization threshold energy of the target the SCOP formalism[52,53] is uded. In this formalism, the electron-molecule system is represented by a

complex optical potential comprising of real and imaginary parts as,

$$V_{opt}(r,E_i) = V_R(r,E_i) + iV_I(r,E_i) \quad (4)$$

such that,

$$V_R(r,E_i) = V_{st}(r) + V_{ex}(r,E_i) + V_p(r,E_i) \quad (5)$$

where, E_i is the incident energy. Eq. 5 corresponds to various real potentials to account for the electron target interaction namely, static, exchange and the polarization potentials respectively. These potentials are obtained using the target geometry, molecular charge density of the target, the ionization potential and polarizability as inputs. The molecular charge density is derived from the atomic charge density by expanding it at the center of mass of the system. The molecular charge density so obtained is normalized to account for the total number of electrons present in the target. The atomic charge densities and static potentials (V_{st}) are formulated from the parameterized Hartree-Fock wave functions given by Cox and Bonham[54].

The parameter free Hara's 'free electron gas exchange model'[55] is used for the inclusion of exchange potential (V_{ex}). The exchange potential takes care of exchange of scattering electron with one of the target electrons. The polarization potential (V_p) is formulated from the parameter free model of correlation-polarization potential given by Zhang et al. [56]. Here, various multipole non-adiabatic corrections are incorporated in the intermediate region which will approach the correct asymptotic form at large 'r' smoothly. The target parameters like ionization potential (I) and dipole polarizability (α_0) of the target used here are the best available from literature[39].

The imaginary part in V_{opt}, called the absorption potential V_{abs} accounts for the total loss of flux from the incident channel, scattered into the allowed electronic excitation or ionization channels. The expression used here are vibrationally and rotationally elastic. This is due to the fact that the non-spherical terms do not contribute much to the total potential at the present high energy range.

The well-known quasi-free model of Staszeweska et al.[57] is employed for the absorption part, given by,

$$V_{abs}(r,E_i) = -\rho(r)\sqrt{\frac{T_{loc}}{2}}\left(\frac{8\pi}{10k_F^3E_i}\right)\theta(p^2-k_F^2-2\Delta)(A_1+A_2+A_3) \quad (6)$$

Where T_{loc} is the local kinetic energy of the incident electron which is given by,

$$T_{loc} = E_i - (V_{st} + V_{ex} + V_p) \quad (7)$$

Here $p^2 = 2E_i$ and $k_F = [3\pi^2\rho(r)]^{\frac{1}{3}}$ is the Fermi wave vector and A_1, A_2 and A_3 are dynamic functions that depend differently on $\theta(x)$, I, Δ and E_i. These parameters are explicitly given in our earlier publication[58] and hence not repeated here. Here, I is the ionization threshold of the target, $\theta(x)$ is the Heaviside unit step-function and Δ is an energy parameter below which V_{abs} = 0. Hence, Δ is the principal factor which decides the values of total inelastic cross section, since below this value ionization or excitation is not allowed. This is one of the main characteristics of Staszewska model[57]. This has been modified by us by considering Δ as a slowly varying function of E_i around I. Such an approximation is meaningful since Δ fixed at I would not allow excitation at energies $E_i \leq I$. However, if Δ is much less than the ionization threshold, then V_{abs} becomes unexpectedly high near the peak position. The amendment introduced is to give a reasonable minimum value 0.8I to Δ[59] and also to express the parameter as a function of E_i around I, i.e.,

$$\Delta(E_i) = 0.8I + \beta(E_i - I) \quad (8)$$

Here the parameter β is obtained by requiring that Δ = I (eV) at $E_i = E_p$, the value of incident energy at which present Q_{inel} reaches its peak. E_p can be found by calculating Q_{inel} by keeping $\Delta = I$. Beyond E_p, Δ is kept constant and is equal to I.

The complex potential thus formulated is used to solve the Schrödinger equation numerically through partial wave analysis. This calculation will produce unique complex phase shifts for each partial wave which carries the signature of interaction of the incoming projectile with the target. The phase shifts δ_l thus obtained are employed to find the relevant cross sections, total elastic (Q_{el}) and the total inelastic cross sections (Q_{inel}) using the scattering matrix $S_l(k) = exp(2i\delta_l)$ [60,61]. Then the TCS (Q_T) is obtained by adding these two cross sections[60].

We have computed total ionization cross sections using Binary Encounter Bethe (BEB) method[62]. The experimental values of total ionization cross sections (Q_{ion}) are provided by five groups[22–26]. The theoretical estimates of total ionization cross sections are done by two groups[23,27].

3 RESULTS AND DISCUSSION

The present work reports detailed study on electron induced chemistry on CH_3CHO. This includes eigenphase sum, electronic excitations, differential, momentum transfer, ionization, total cross sections and scattering rate coefficients. We have employed ab initio R matrix code below 20 eV. The total cross section is sum of total elastic and total electronic

excitation (inelastic part) cross sections below the ionization threshold of the target. Above the threshold, we have computed the total cross section as the sum of total elastic and total inelastic cross section using the SCOP formalism. Using this composite theory of the two formalisms we are able to predict the TCS over wide energy range from 0.01 eV to 5000 eV.[29,53,58]. The numerical results of total ionization cross sections and TCS for CH_3CHO are reported from threshold to 5000 eV and 0.01 eV to 5000 eV and are listed in Table 4 and Table 5 respectively and are also plotted in figure 7 and 8 respectively.

One of the important tasks of the low energy study is the generation of eigenphase sum as it provides the position and width of resonances which are important features of collision study. Resonances are a common characteristic of electron molecule scattering at low impact energies and leads to distinctive structure in pure vibrational excitation cross sections[63] leading to knowledge of decay channels of the target. A recursive procedure for detecting and performing Breit Wigner fits[48] to the eigenphase diagram is done through program RESON[49]. This program generates new energy points and marks those points where the numerically computed values of second derivative changes sign from positive to negative. Finer grids are constructed about each of these points which are used as inputs for Briet Wigner fit[48] and two most important parameters (Position and width) related to resonances are obtained.

Table 3 gives the positions and widths of resonances obtained in the present case using R-matrix calculations. Temporary negative ions in general cause structure in the inelastic cross-sections, and the energy dependence of the various inelastic processes thus represent a convenient way to obtain a global view of the negative ion states. Table 3 shows the resonances detected in A' and A" symmetries using cc-pVDZ, DZP and 6-31G basis sets in our calculations and are shown graphically in Figure 1. Doublet A" state shows a shape resonance structure at 1.33 eV with a resonance width of 0.1726 eV using DZP basis set. Our value is in excellent agreement with measured data of 1.3 eV reported by van Veen et. al.[7], 1.19 eV reported by Jordan et. al.[8] and 1.20 eV reported by Dressler & Allan[10] and comparable with theoretical prediction of 1.65 eV by Gauf et. al.[20]. This resonance is reflected as a strong peak in the TCS curve exactly at 1.3 eV with a maximum cross section value of 166.4 $Å^2$ shown in INSET (1) of Fig. 8. No experimental data reflects this resonance peak in TCS curve. Second resonance obtained in 2A" state is at 2.78 eV and 2.43 eV using cc-pVDZ and 6-31G basis sets respectively for which no comparisons are available. Third resonance predicted by 2A' symmetry is at 4.14 eV with a broad width of 3.60 eV. We do not find any

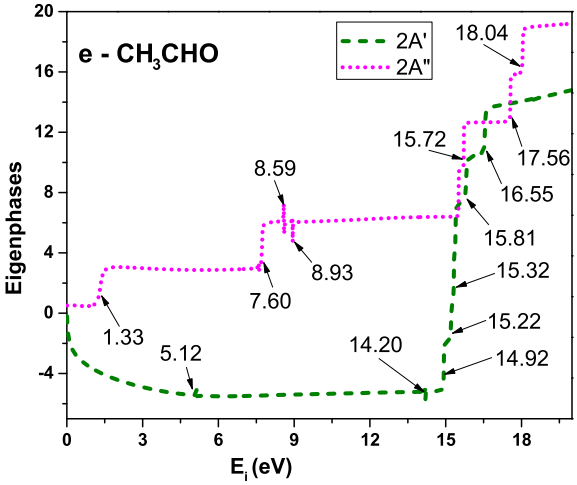

Fig. 1 (color online): Eigenphase diagram; Short dash - 2A' symmetry, Short dot - 2A" symmetry

comparison for this resonance. The other resonance observed at 7.6 eV using DZP basis set is analogous to Feshbach resonances predicted by Dressler and Allan[10] at 6.34 eV, 6.64 eV and 6.80 , at 6.5 eV and 6.6 eV by Szymanska et. al.[18] and at 6.0 eV by Dorman[16]. This resonance is responsible for fragments CH_3^-, CH_3CO^- predicted by[10,16,18]. We observe two resonances at 8.59 eV and 8.94 eV due to 2A' symmetry using DZP basis set. The 8.59 eV resonance is in excellent agreement with 8.60 eV reported by Szymanska et. al.[18] and it is responsible for C_2H^- fragment. Similarly our resonance at 8.94 eV is in good agreement with resonances predicted at 9.00 eV and 9.4 eV by Dorman et. al.[16] and at 9.2 eV reported by Szmynska et. al.[18] and Dressler and Allan[10]. These resonances are responsible for O^- C_2HO^-, CH_3CO^-, OH^- fragments. We also observed a Feshbach resonance at 10.03 eV and 10.34 eV for A' symmetry using cc-pVDZ and 6-31G basis set respectively which are in excellent agreement with theoretical value of 10.30 eV by Biery et. al.[64], 10.26 eV by Kimura et. al.[65] and measured value of 9.9 eV and 10.00 eV by Szymanska et. al.[18] and at 10.0 eV by Dorman [16].This resonance is responsible for fragments CH_2^-, C_2H^- and O^- predicted by[16,18]. This resonance is also reported at 9.5 eV by Prabhudesai et. al.[66]. For resonances above 10 eV we do not find any comparison and hence reported here for the first time. Figure 1 shows eigenphase diagram obtained using DZP basis sets and all resonances discussed above are seen in this figure. Thus the eigenphase study provides us a detailed knowledge about fragmentation of acetaldehyde.

Figure 2 presents electron-impact excitation cross sections

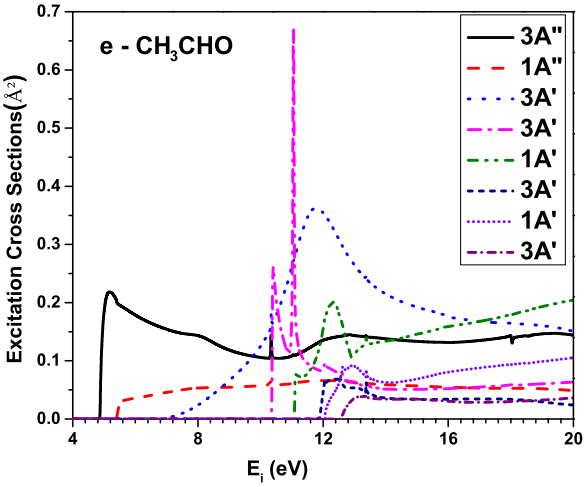

Fig. 2 (color online):Excitation cross sections from the ground state (X 1A') to the first eight excited states; Solid - 3A", Dash - 1A", Dot - 3A', Dash dot - 3A', Dash dot dot - 1A', Short Dash - 3A', Short dot - 1A', Short dash dot - 3A'

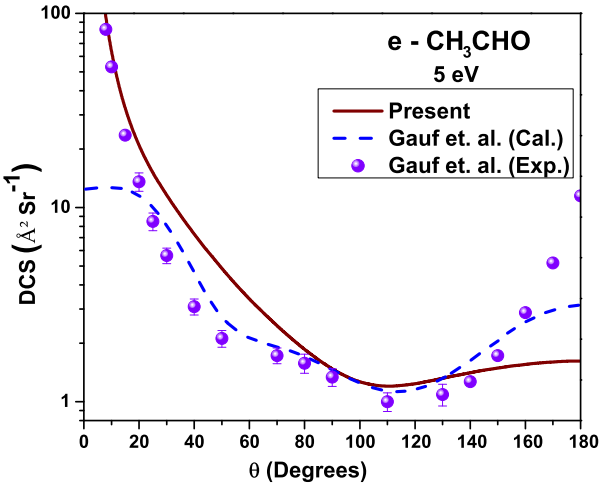

Fig. 3 (color online): Rotationally resolved Differential Cross Sections (DCS) for incident energy of 5 eV; Present - Solid line; Gauf et. al.[20]: Dash line - Calculations, Solid Sphere - Experiment

from the ground state (X 1A') to the first eight excited states (3A", 1A", 3A', 3A',1A', 3A', 1A' and 3A') for impact energies 0 to 20 eV obtained using R-matrix calculation. The first electronic excitation energy is 4.88 eV which is obtained from the transition of ground state of X 1A' to 3A". This value of first electronic excitation is close to 4.38 eV reported in[35] and 4.3 reported by Walsh[36] and 4.49 eV reported by Wiberg et. al.[47]. The excitation cross section for this transition rises sharply with maximum value of 0.22 $Å^2$ and then decreases slowly and shows a structure at around 12 eV. The other important transition is from ground state X 1A' to 3A' which starts nearly at 10.4 eV and rises sharply to maxima of 0.67 $Å^2$. This transition is analogous to electronic excitations predicted at 9.51 eV by Tam and Brion[12], at 9.5 eV predicted by Walsh[36] and at 9.4 eV by Van veen et. al.[7]. The third important electronic transition is from ground state X 1A' to 3A' which starts around 6 eV, attains abroad peak at 12 eV with its maximum cross section value of 0.35 $Å^2$ and slowly diminishes to 0.15 $Å^2$ at 20 eV.

This transition is analogues to earlier predictions of 6.88 eV by Wiberg et. al. and 6.82 eV and 6.97 eV by Tam and Brion[12] and Walsh[36] respectively. Beyond 13 eV the contribution to excitation cross section from all channels diminishes. These cross sections show the probability of excitation to various energy levels of the target.

Figure 3 shows comparison of our rotationally resolved DCS at 5 eV for the sum total of all transitions (J = 0 to J'= 0

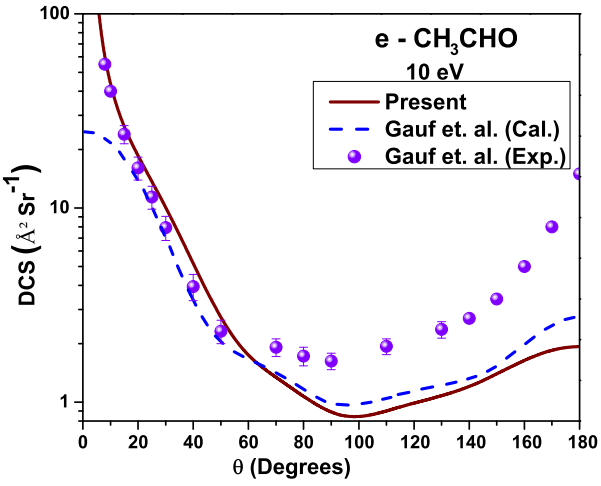

Fig. 4 (color online): Rotationally resolved Differential Cross Sections (DCS) for incident energy of 10 eV; Present - Solid line; Gauf et. al.[20]: Dash line - Calculations, Solid Sphere - Experiment

to 5) compared with experimental and theoretical results of Gauf et. al.[20].There is no other theoretical or experimental comparison to the best of our knowledge. The total DCS at 5 eV is dominated by the dipole component (J = 0 → J' = 1). As CH_3CHO is a polar molecule, the dipole component (J = 0 → J' = 1) is much larger than the elastic component (J = 0 → J' = 0). The calculated DCS is converged when J' increases up to 5. Moreover, in the elastic component, there is a minimum at about 110° which coincides with theoretical minima of Gauf et al.[20]. We do not observe minimum at 50° as observed in theoretical results as well as experimental results of Gauf et. al.[20]. Present data is in good agreement with experimental data of Gauf et. al.[20] except beyond 140° where they have extrapolated their DCS results.

Figure 4 shows sum of our rotationally resolved differential cross sections summed over all transitions (J=0 to J'= 0 to 5) for incident energy of 10 eV compared with measured and theoretical results of Gauf et. al.[20]. The scattering is dominated by elastic component 0 → 0 and dipole component 0 → 1. The elastic component shows a strong dip around 100° which indicates the dominance of a p-wave in the interference pattern arising due to various partial wave amplitudes. As the energy increases the convergence with respect to J is rapid. The divergence at the forward angle is confirmed as being due to dipole allowed transitions 0→1 dominating the scattering. The DCS decrease as the incident energy increases. The sharp enhancement in the forward direction is a result of the strong long-range dipole component of the interaction potential. Our data finds very good agreement with theoretical and experimental data of Gauf et. al.[20] for low angles up to 80° and the minima position also matches for both the results. Quantitatively our data differs from both theoretical and experimental values of Gauf et. al.[20] above 80° and this may be due to extrapolation of their results beyond 135°.

Figure 5 shows sum of our rotationally resolved differential cross sections summed over all transitions (J=0 to J'= 0 to 5) for incident energy of 15 eV compared with measured and theoretical results of Gauf et. al.[20]. The elastic component shows a shallow dip around 90°. Present data finds very good agreement with theoretical as well as experimental data of Gauf et. al.[20] for all angles below 100° above which theoretical data find good match while experimental values are qualitatively good but varies quantitatively. This variation in experimental data may be attributed to the extrapolation error beyond 130°.

The Momentum Transfer Cross Sections (MTCS) indicates the importance of the backward scattering and is an important quantity that forms the input to solve the Boltzmann equation for the calculation of electron distribution function of swarm

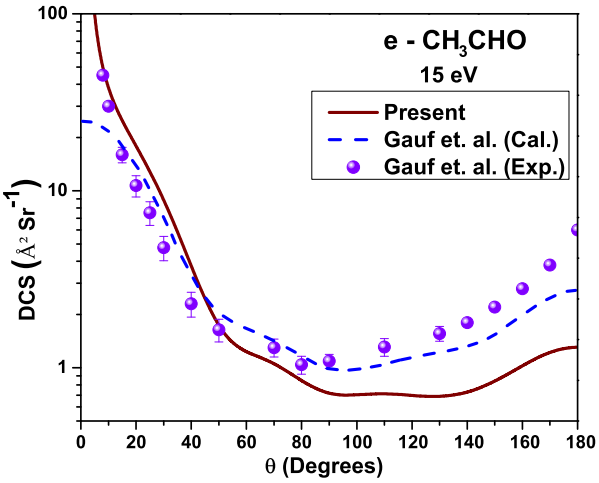

Fig. 5 (color online): Rotationally resolved Differential Cross Sections (DCS) for incident energy of 15 eV; Present - Solid line; Gauf et. al.[20]: Dash line - Calculations, Solid Sphere - Experiment

of electrons drifting through a molecular gas. The divergent behavior observed in DCS in the forward direction, the divergence in MTCS is reduced due to the multiplicative factor (1 - cosθ). A further test of the quality of our DCS is shown by the MTCS in figure 6 from energies 0 eV to 20 eV. We have compared our MTCS data with theoretical and experimental data of Gauf et. al.[20]. The various peaks or structures observed in MTCS correspond to various resonance processes. There are large number of fragmentation possible of acetaldehyde below 20 eV[18]. We get signature of these fragmentations in the MTCS curve in the form of peaks/structures. We have performed CAS-CI calculations using two target models viz. CAS=3, number of states per symmetry, n=1 and R matrix radius r=12 (c3n1r12) and (c7n5r13).The first distinct peak observed at 2.5 eV with peak momentum transfer cross section value of 38.87 $Å^2$ using c7n5r13 model and at 2.58 eV with peak value of 40.1 $Å^2$ using c3n1r12 are comparable with similar peak reported by Gauf et. al.[20] at 1.6 eV with peak value of momentum transfer cross section of 41.89 $Å^2$.

Table 3 Position and width of resonance states along with fragment ions of CH_3CHO

State	Position			Width			Other Position (eV)		Anionic Fragments
	cc-pVDZ	6-31G	DZP	cc-pVDZ	6-31G	DZP	Theoretical	Experimental	
2A'		4.14			3.6016				
	9.60			0.0132				9.90[18]	C_2H^-
	10.03	10.34		0.0688	0.0182		10.30[64]	10.00[16]	CH_2^-
							10.26[65]	10.00[18]	O^-
		11.05			0.0503				
			14.20			0.0023			
			14.92			0.0111			
			15.22			0.0528			
			15.32			0.0117			
			15.80			0.0476			
			16.55			0.0312			
		17.59			1.4580		-	-	
2A"			1.33			0.1726	1.65[20]	1.30[7]	
								1.20[10]	
								1.19[8]	
	2.78	2.43		0.5200	0.3903				
			7.60			0.0030		6.80[10], 6.64[10], 6.60[18]	CH_3^-
								6.50[18], 6.34[10]	CH_3CO^-
								6.00[16]	CH_3^-, CH_3CO^-
			8.59			0.0145		8.60[18]	C_2H^-
			8.94			0.0061		9.00[16]	OH^-, CH_3CO^-
								9.40[16]	O^-
								9.20[16,18]	C_2HO^-
	12.33	12.95		0.0072	0.0933				
			15.72			0.0082			
	17.85		17.56	0.0354		0.0093			
	18.11	18.03	18.04	0.0823	0.0308	0.0221	-	-	
		18.57			0.0939				

This resonance peak corresponds to π^* shape resonance due to capture of incoming electron into the π^* A_2 orbital state. We observed another peak at 10.37 eV of magnitude 18.8 $Å^2$ which may be due to CH_2^- fragment as reported by Dorman et. al.[16] and Bieri et. al.[64] at 10.00 eV and 10.30 eV respectively and fragment O^- as reported by Kimura et. al.[65] and Szymanska et. al.[18] at 10.26 eV and 10.00 eV respectively. There exist some deviation between our results and the experimental and theoretical data of Gauf et. al.[20].

Electron impact total ionization cross section is the most important fundamental quantity to many areas of applied interest. It is used as basic calibration data for a variety of analytical instruments such as ionization manometers, ionization chambers and mass spectrometers. Furthermore these quantities have the same basic significance for the initiation of reactions by ionizing radiation as do absorption coefficients for photo-chemical reaction initiation. In figure 7, we report comparison of our total ionization cross section for e - CH_3CHO scattering with available results. We have calculated total ionization cross sections using Binary Encounter Bethe (BEB) method[62]. The numerical values of total ionization cross sections are provided in table 4. Our data finds excellent agreement with measured data of Bull and Harland[22] for all impact energies reported by them and also with single predicted data at peak of ionization cross sections reported by Beran and Kevan[24] and Otvos and Stevenson[26]. Our data finds very good agreement with theoretical values of Gupta and Antony[27] and also with theoretical data of Vacher et. al.[23] except at the peak where their values[23] are lower than our data. The measured values reported by Vacher et. al.[23] is in good agreement with our data up to 25 eV above which they are significantly lower compared to all data reported here except that of Harrison et. al.[25] which is also very low. The reason for lower value of ionization cross sections reported by Vacher et. al.[23] is that they have measured partial ionization cross section for only two fragments of CH_3CHO, HCO^+ and CH_3CO^+ viz. The contributions from other fragments is not considered by Vacher et. al.[23] and hence the lower ionization cross sections are justified. Thus our data finds good agreement with most of the theoretical[23,27] as well as experimental[22–26] data.

It is a regular observation that due to the presence of long range dipole interaction, the total cross section at low energy is diverging in the fixed nuclei approximation owing to singularity in the differential cross section in the forward direction. It is well known that the cross sections of dipole dominated processes only converge slowly with partial waves due to long range nature of the dipole potential. To obtain converged cross sections, the effect of rotation must be included along with a large number of partial waves. The higher partial waves (l $\geq$ 4) are included using a Born correction as given in the work of Chu and Dalgarno[67]. This is done by adjusting the T-matrices using the Close Coupling "CC" cross sections generated by the code POLYDCS[50]. In this procedure our low l T-matrices are added to analytic dipole Born T- matrices using the adiabetic nuclear rotation (ANR)[68,69]. The Born contribution for partial waves higher than $l = 4$ to the elastic cross section at energies below 1.5 eV is quite large as seen from Fig. 8.

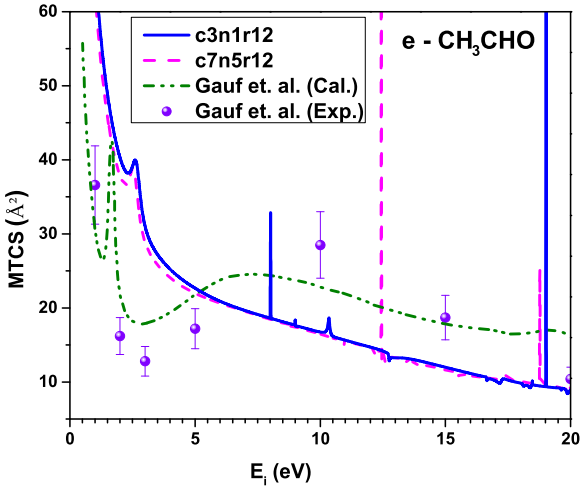

Fig. 6 (color online): Momentum Transfer Cross Section (MTCS); Present: Solid line - c3n1r12, Dash line - c7n5r12 (See text), Gauf et. al.[20]: Dash dot dot line - Calculations, Solid sphere - Experiment

In figure 8, we have compared total cross sections data for e $-$ CH_3CHO scattering using 6-31G, DZP and cc-pVDZ basis sets with available comparisons. The significant structures observed in TCS using DZP basis set are shown in INSET (1) and INSET (2) of Fig. 8. The total cross section calculation depends on the target model which in turn depends on R-matrix radius (r), Number of states per symmetry (n) and Complete Active Space (c) considered in present calculations. We performed series of calculations and finalised two target models for computation of total cross section using two different basis sets viz. 6-31G (Model 1 (M1) - c5n10r13)and cc-pVDZ (Model 2 (M2) - c3n8r12). We have taken the R-matrix radii to be 12 au and 13 au and observed the consistency of results. With increase of the R-matrix radius, the cross section value increases which is evident from figure 8. Increasing the CAS value, the computation becomes more complex and time consuming and it will make the resonant structures more refined but do not change the magnitude of the results to larger extent. Finally increasing the number of states per symmetry will increase the computational time and

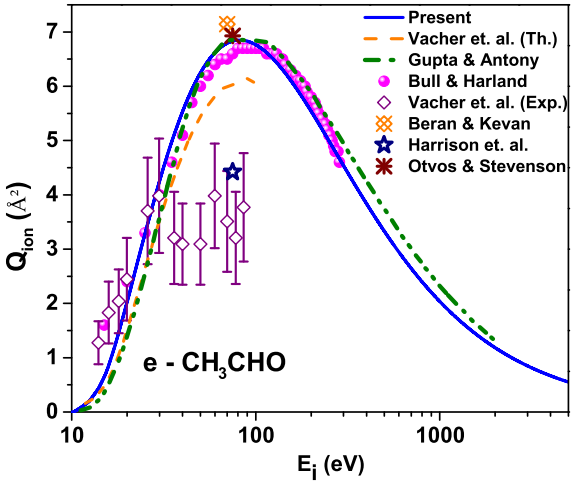

Fig. 7 (color online): Total Ionization Cross Sections; Present BEB calculations - Solid line; Other theoretical data: Dash line - Vacher et. al.[23], Dash dot dot line - Gupta & Antony[27]; Other Experimental data: Solid sphere - Bull & Harland[22], Open Dimond - Vacher et. al. [23], Crossed Diamond - Beran & Kevan[24], Open Star - Harrison et. al.[25], Asterisk - Otvos & Stevenson[26]

will shift the peak value of cross sections towards left as can be seen from figure 8.

The prominent structures observed in the total cross section curve presented for e - CH_3CHO scattering is shown in Figure 8. Many structures and peaks observed in our eigenphase sum, momentum transfer curve and excitation curves are averaged out in total cross section curve. We observed two prominent peaks in our TCS curve. The first peak is a shape resonance observed at 1.3 eV with peak value of cross section of 166.4 $Å^2$ while that reported by theoretical value of Gauf et. al.[20] is at 1.6 eV with magnitude of cross section being 63.31$Å^2$. Our shape resonance is in very good agreement with experimental peak reported at 1.19 eV[8], 1.20 eV[10] and 1.3 eV[7] and theoretical peak at 1.65 eV[20]. This peak is shown in INSET (1) of figure 8. Shape resonance structure at low energy is not observed in the measured data of Szmytkowski et. al.[21] and also in measured data of Gauf et. al.[20] as their reported experimental data is from 3 eV onwards.

The second peak is a broad maximum which is from 6 eV to 15 eV observed in all the results presented here having different value of position of the peak. The peaks obtained using DZP basis set in TCS curve are shown in inset2 of the TCS figure 8. It shows peaks at 5.14 eV with peak value of 44.42 $Å^2$, 7.61 eV with peak value of 39.42 $Å^2$, at 7.72

Table 4 Total ionization Cross Sections

E_i (eV)	Q_{ion} ($Å^2$)	E_i (eV)	Q_{ion} ($Å^2$)	E_i (eV)	Q_{ion} ($Å^2$)
10.3	0.01	100	6.76	1000	2.04
20	2.02	200	5.54	1500	1.49
30	4.26	300	4.54	2000	1.18
40	5.53	400	3.84	2500	0.99
50	6.24	500	3.33	3000	0.85
60	6.62	600	2.95	3500	0.75
70	6.79	700	2.64	4000	0.67
80	6.85	800	2.40	4500	0.60
90	6.83	900	2.20	5000	0.55

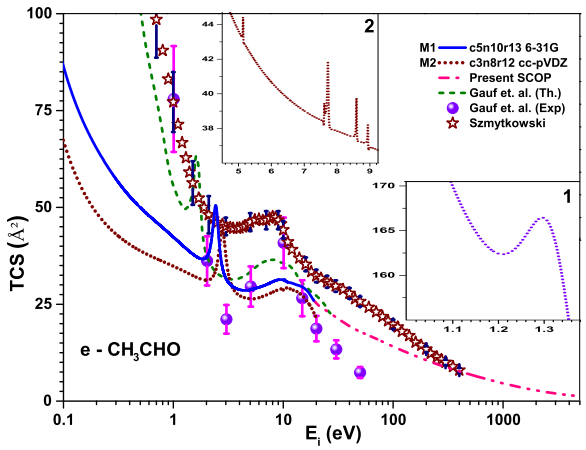

Fig. 8 (color online): e - CH_3CHO Total Scattering Cross Sections; Calculations: Present R-matrix: Solid line - Model 1 (M1), Short Dot line - Model 2(M2) see the text, Present SCOP - Dash dot dot line, Short Dash line - Gauf et. al.[20]; Experiment: Solid Sphere - Gauf et. al.[20], Open Star - Szmytkowski[21]
INSET (TCS calculated using DZP basis set): (1) 1 eV to 1.4 eV (2) 5 eV to 9 eV

eV with peak value of 41.31 $Å^2$, 8.59 eV with peak value of 39.73 $Å^2$ and at 8.94 eV with peak value of 38.2 $Å^2$. These peaks corresponds to various fragmentation of acetaldehyde as discussed in our resonance table 3. Our cc-pVDZ basis set results have peak at 10.31 eV with peak value of TCS as 29.48 $Å^2$ while theoretical data of Gauf et. al.[20] have peak at 8.54 eV with peak value of 36.4 $Å^2$ and their measured data reports peak at 10.11 eV with magnitude of integral cross section as 40.99 $Å^2$ and Szmytkowski et. al.[21] reports their peak at 8.38 eV with peak value of 47.55 $Å^2$. There are many fragments reported between 6 and 12 eV by Szymanska et. al. [18] and this may be the reason for having broad peak around 10 eV. The broad maximum in the Integral Cross Sections (ICS) near 10 eV results from overlapping 2A' and 2A" features, each of which may contain more than one broad resonance as

Table 5 Total Cross Section ($\AA^2$) for the e - CH_3CHO Scattering

E_i (eV)	R- matrix	E_i (eV)	R- matrix	E_i (eV)	R- matrix	E_i (eV)	SCOP	E_i (eV)	SCOP
0.01	583.16	1.6	37.39	8.0	30.82	19	25.19	600	6.25
0.05	134.10	1.8	36.70	8.5	31.12	20	25.13	700	5.72
0.1	86.36	2.0	37.09	9.0	31.31	30	21.66	800	5.28
0.2	65.25	2.5	48.17	9.5	31.36	40	19.25	900	4.90
0.3	57.35	3.0	31.72	10.0	31.27	50	17.92	1000	4.58
0.4	52.85	3.5	29.50	11.0	30.65	60	16.94	1500	3.44
0.5	49.95	4.0	28.77	12.0	30.51	70	16.10	2000	2.76
0.6	47.87	4.5	28.55	13.0	30.06	80	15.34	2500	2.30
0.7	46.20	5.0	28.75	14.0	29.81	90	14.66	3000	1.97
0.8	44.77	5.5	29.05	15.0	29.49	100	14.06	3500	1.72
0.9	43.49	6.0	29.36	16.0	28.88	200	10.47	4000	1.53
1.0	42.33	6.5	29.69	17.0	28.08	300	8.77	4500	1.37
1.2	40.30	7.0	30.05	18.0	26.98	400	7.69	5000	1.25
1.4	38.64	7.5	30.44	-	-	500	6.88	-	-

Table 6 Functional Group Study

Target	Molecular Formula	IP eV	No. of electrons	Dipole moment[37] (μ) in D	Bondlength ($\AA$)[37] C=O	C-R	Polarizability (α)[37] $\AA^3$
Acetaldehyde	CH_3CHO	10.229	24	2.69	1.216	1.501	4.278
Formaldehyde[28]	HCHO	10.885	16	2.33	1.205	1.111	2.77
Formic Acid[28]	HCOOH	11.33	24	1.41	1.202	1.343	3.319
Formamide[29]	$HCONH_2$	10.16	24	3.73	1.21	1.35	4.2
Ethylene Oxide	H_2COCH_2	10.56	24	1.89	1.425	1.459	4.43

confirmed through theoretical data[20]. Our results are in very good agreement with measured data of Gauf et. al.[20] between 3 eV and 20 eV beyond which our data are higher than their values. The measured data of Szmytkowski et. al.[21] are much higher than our values below 200 eV above which they slowly merge with our values. It is interesting to note that there is smooth transition at overlap energy between our data reported using two formalisms (R-matrix and SCOP). There are no theoretical or experimental data reported above 400 eV to the best of our knowledge.

In Fig. 9 we present the comparison of total cross section of CH_3CHO with other structurally similar (HCHO) and isoelectronic targets ($HCOOH$[28], $HCONH_2$[29] and H_2COCH_2[30] as the comparison for its total cross sections is very limited. Due to the scarcity of TCS data on elastic scattering by acetaldehyde, results for these isoelectronic and structurally similar analogs are useful points of comparison and also to understand the effect of functional groups on the structures observed at low energy. Resonance effect depends on the valence bonding order, an electron negativity of atoms as well as the molecular geometry. Table 6 shows the comparison of various target properties of these targets. All these compounds contain the $\pi*$ unoccupied orbital on the C=O bond which is responsible for a shape resonance. And we find the

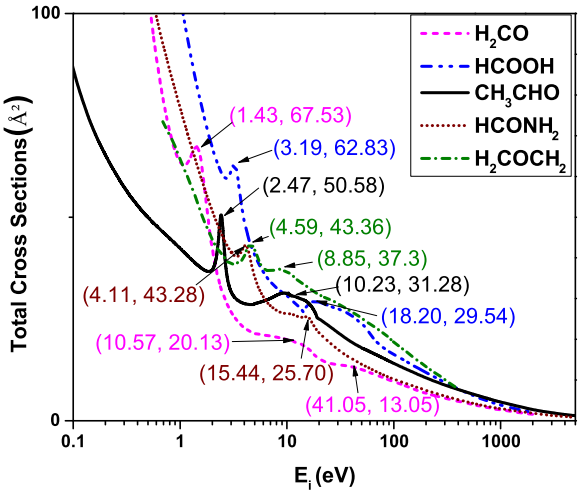

Fig. 9 (color online)Effect of Functional group on electron impact Total Cross Sections; Solid - H_2CO[28], Dash dot dot - $HCOOH$[28], Short dash - CH_3CHO, Short dot - $HCONH_2$[29], Short dash dot - H_2COCH_2[30]

presence of shape resonance in all the targets compared here. Replacing the CH_3 group in formaldehyde by a hydrogen atom is expected to lower the energy of the resonance since the CH_3 group donate electrons to the carbonyl chromophore more efficiently than an H atom. This is observed since our shape resonance peak for acetaldehyde is at 2.47 eV while that for formaldehyde is at 1.43 eV. Our second observation is that ethylene oxide and formamide have almost same peak position (4.59 eV and 4.11 eV) and magnitude (43.36 $\AA^2$ and 43.38 $\AA^2$) of total cross section respectively. Similar observation is also for formaldehyde and formic acid where their peak positions differs as 1.43 eV and 3.19 eV and peak values are comparable 67.53 $\AA^2$ and 62.83 $\AA^2$ respectively. The shift in peak position may be attributed to size of the functional group. The second important observation is that all these molecular targets show second peak in their TCS curve and they are due to $\sigma*$ shape resonance. This resonances are all observed between 10 eV and 20 eV. The position of their second peak is at 10.57 eV, 18.20 eV, 10.23 eV, 15.44 eV and 8.85 eV for H_2CO, $HCOOH$, CH_3CHO, $HCONH_2$ and H_2COCH_2 respectively. Further all these targets are polar in nature and that is reflected by a sharp rise (divergence)in the TCS curve at low energies. At higher energies beyond 300 eV the TCS from all these targets tend to merge implying that at these energies they do not depend on structure but depend on size of the target and the effective interaction time between the target and the electron. As energy increases the effective time of interaction decreases and hence the cross sections also decreases.

Finally electron impact scattering rate coefficients are plotted as a function of the kinetic temperature which is defined according to the Maxwell Boltzmann distribution. From this graph it is noted that the scattering rate increases rapidly up to approximately 300 K before gradually dying down as the temperature is further increased. The maximum rate coefficient value is 6.23 $\times$ 10^{-6} cm^3/s at 320 eV. There is no data for comparison to the best of our knowledge.

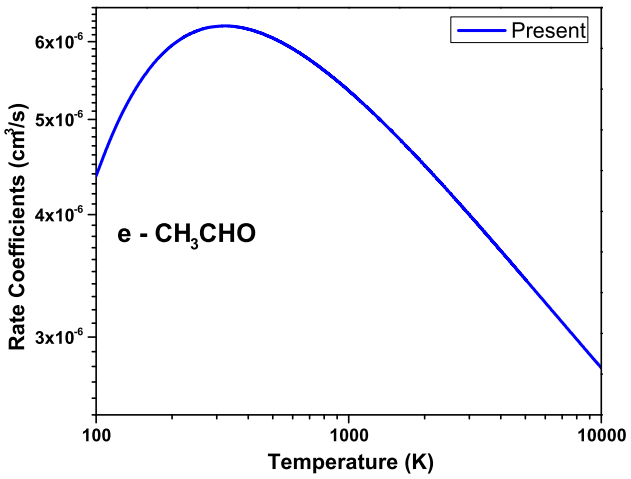

Fig. 10 (color online): total rate coefficients for e - CH_3CHO elastic scattering

4 Conclusion

We report comprehensive study of electron impact on acetaldehyde over an extensive range of impact energies. We employed ab initio R-matrix calculations for impact energies below 20 eV and above it spherical complex optical potential is used. We employed fixed nuclei close coupling formalism with static exchange plus polarization model using 6-31G, DZP and cc-pVDZ basis sets. The target properties computed using quantum chemistry codes provide good target properties as evident from Table 1. The eigenphase diagram predicts resonance peak and width which are reported in Table 3 and the fragmentation observed due to this resonances are in accordance with earlier literature [7,8,10,16,18,64,65] . Present DCS and ionization cross section find good agreement with earlier reported data. At low energy the total cross section shoots up due to dipole potential. We observe $\pi*$ shape resonance at 1.33 eV which arises as scattering electron occupies the vacant $\pi*$ orbital of carbonyl group (C=O). This resonance is in excellent agreement with peak at 1.3 predicted experimentally van Veen et. al.[7], 1.19 eV by Jordon and Burrow[8] and 1.2 eV reproted by Dressler and Alan[10]. There is no theoretical TCS data beyond 30 eV and experimental data beyond 400 eV of the total cross sections and hence reported for the first time. The scattering rate coefficients are also reported for the first time. The maximum rate coefficient value is 6.23 $\times$ 10^{-6} cm^3/s at 320 eV. Due to sparse data for total cross sections we also reported comparison of total cross section of acetaldehyde with its structurally similar and isoelectronic targets. Finally our theory is able to predict the possible neutral fragmentation of Acetaldehyde which are listed in Table 3 that are difficult to predict using mass spectrometry. The present work will inspire both theoreticians as well as experimentalist to investigate all the features for e - CH_3CHO scattering reported in this paper.

5 Acknowledgement

Minaxi Vinodkumar and Chetan Limbachiya acknowledge DAE-BRNS, Mumbai for the Major research project [37(3)/14/44/BRNS-2014] for financial support under which part of this work is carried out.

References

1 C. A. Gottlieb, in Molecules in the Galactic Environment, edited by M. A. Gordon and L. E. Snyder (Wiley-Interscience, New York, 1973), pp. 181186.

2 N. Fourikis, M. W. Sinclair, B. J. Robinson, P. D. Godfrey, and R. D. Brown, Aust. J. Phys., **27**, 425 (1974).

3 W. Gilmore, M. Morris, D. R. Johnson, F. J. Lovas, B. Zuckerman, B. E. Turner, and P. Palmer, Astrophys. J., **204**, 43 (1976)

4 W. Gilmore, M. Morris, and D. R. Johnson, ApJ, **204**, 43 (1976).

5 H. Matthews, P. Friberg and W. Irvine, ApJ, **290**, 609 (1985).

6 Nummelin, P. Bergman, and A. Hjalmarson et al., ApJS 128, p. 213 (2000).

7 E. H. van Veen, W. L. van Dijk, and H. H. Brongersma, Chem. Phys., **16**, 337 (1976).

8 K. D. Jordan and P. D. Burrow, Acc. Chem. Res., **11**, 341 (1978).

9 C. Benoit, R. Abouaf, and S. Cvejanovic, Chem. Phys., **117**, 295 (1987).

10 R. Dressler and M. Allan, J. Electron Spectrosc. Relat. Phenom., **41**, 275 (1986).

11 W. T. Naff, R. N. Compton, and C. D. Cooper, J. Chem. Phys., **57**, 1303 (1972).

12 W.-C. Tam and C. E. Brion, J. Electron Spectrosc. Relat. Phenom., **3**, 467 (1974).

13 R. H. Staley, L. B. Harding, W. A. Goddard, III, and J. L. Beauchamp, Chem. Phys. Lett., **36**, 589 (1975).

14 T. Ari and J. B. Hasted, Chem. Phys. Lett., **85**, 153 (1982).

15 K. N.Walzl, C. F. Koerting, and A. Kuppermann, J. Chem. Phys., **87**, 3796 (1987).

16 F. H. Dorman, J. Chem. Phys., **44**, 3856 (1966).

17 R. Dressler and M. Allan, Chem. Phys. Lett., **118**, 93 (1985).

18 E. Szymanska, V. S. Prabhudesai, N. J. Mason, and E. Krishnakumar, Phys. Chem. Chem. Phys., **15**, 998 (2013).

19 E. Burean and P. Swiderek, J. Phys. Chem. C , **112**, 19456 (2008).

20 A. Gauf, C. Navarro, G. Balch, L. R. Hargreaves, and M. A. Khakoo, Phys. Rev. A, **89**, 022708 (2014).

21 C. Szmytkowski, J. Phys. B, **43**, 055201 (2010).

22 J. Bull and P. Harland, Int. J. Mass Spect., **273**, 53 (2008).

23 J. Vacher , F. Jorand, N. Blin-Simiand, S. Pasquiers, Chemical Physics **323**, 587 (2006).

24 J. Beran and L. Kevanl, J. Phys. Chem., **73 (11)**, 3866 (1969).

25 Canadian Journal of Chemistry., A. Harrison, E. Jones, S. Gupta and G. Nagy, **44**, 1967 (1966).

26 J. Otvos and P. Stevenson, J. Am. Chem. Soc., **78**, 546 (1956).

27 D. Gupta and B. Antony, J. Chem. Phys., **141**, 054303 (2014).

28 M. Vinodkumar, H. Bhutadia, B. Antony and N. Mason, Phys. Rev. A, **84**, 052701 (2011).

29 M. Vinodkumar, C. Limbachiya, H. Desai and P.C. Vinodkumar, J. App. Phys. **116**, 124702 (2014).

30 C. Szmytkowski, A. Domaracka, P. Mozejko and E. Ptasinska-Denga, J. Phys. B: At. Mol. Opt. Phys. **41**, 065204 (2008).

31 J. Tennyson, J. Phys. B: At. Mol. Opt. Phys. **29**, 6185 (1996).

32 D. Bouchiha, J. D. Gorfinkiel, L. G. Caron, and L. Sanche, J. Phys. B: At. Mol. Opt. Phys. **40**, 1259 (2007).

33 A. Jain, and K.L. Baluja, Phys. Rev. A **45**, 202 (1992).

34 J. Tennyson, Physics Reports **491**, 29 (2010).

35 `http://www.gaussian.comg_techg_urk_scrf.html`

36 A.D. Walsh, Proc. Roy. Soc. London A **185** 176 (1946).

37 `http://cccbdb.nist.gov`

38 Paul H. Turner and A. Peter Cox , J. Chem. Soc. Faraday Trans. 2, **74**,533 (1978).

39 Handbook of Chemistry and Physics, 87th ed., edited by D. R. Lide (CRC,Boca Raton, FL, 2007).

40 R. D. Nelson Jr., D. R. Lide, A. A. Maryott "Selected Values of electric dipole moments for molecules in the gas phase" NSRDS-NBS10, 1967.

41 Maria A. M. Cordeiro and Joao M. M. Cordeiro, J. Braz. Chem. Soc., **15 (3)**, 351 (2004).

42 B.Sarpal, K. Pfingst, B. Nestmann and S. Peyerimhoff, J. Phys. B: At. Mol. Opt. Phys. **29**, 857 (1996).

43 'Computational Methods for Electron Molecule Collisions',edited by W. M. Huo and F. A. Gianturco (Plenum, New York,1995).

44 B. I. Schneider and T. N. Rescigno, Phys. Rev. A 37, 3749 (1988).

45 T. N. Resigno, C.W. McCurdy, A. E. Orel, and B. H. Lengsfield III, in Computational Methods for Electron Molecule Collisions, edited by W. M. Huo and F. Gianturco (Plenum, New York,1995), pp. 144

46 E Joucoski and M H F Bettega, J. Phys. B: At. Mol. Opt. Phys. **35**, 783 (2002)

47 K. Wiberg, R. Stratmann and M. Frisch, Chem. Phys. Lett. **297**, 60 (1998).

48 J. Tennyson and C. J. Nobel, Comput. Phys. Commun. **33**, 421(1984).

49 J. Tennyson, C.J. Noble, Comput. Phys. Comm. **33**, 421(1984).

50 N. Sanna and F. A. Gianturco, Comput. Phys. Commun. **114**, 142 (1998).

51 F. A. Gianturco and A. Jain Phys. Rep. **143**, 347 (1986).

52 A. Jain, and K.L. Baluja, Phys. Rev. A **45**, 202 (1992).

53 M. Vinodkumar, H. Desai and P.C. Vinodkumar, RSC Adv., **5**, 24564 (2015).

54 H. L. Cox, and R. A. Bonham, J. Chem. Phys. **47**, 2599 (1967).

55 S. Hara, J. Phys. Soc. Japan **22**, 710 (1967).

56 X. Zhang, J. Sun, and Y. Liu, J. Phys. B: At. Mol. Opt. Phys. **25**, 1893 (1992).

57 G. Staszewska, D. W. Schewenke, D.Thirumalai, and D. G. Truhlar, Phys. Rev. A **28**, 2740(1983).

58 M. Vinodkumar, C. Limbachiya, H. Desai and P.C. Vinodkumar, Phys. Rev. A **89**, 062715 (2014).

59 M. Vinodkumar, K. Korot, P.C. Vinodkumar, Int. J. of Mass Spectrometry **305**, 26 (2011).

60 C. J. Joachain, Quantum Collision Theory (Amsterdam: North-Holland) (1983).

61 Minaxi Vinodkumar and Mayuri Barot, J. Chem. Phys. **137**, 074311 (2012).

62 Y. Kim and M. Rudd, Phys. Rev. A **50** 3954 (1994).

63 L. Andric, I. M. Cadez, R. I. Hall, and M. Zubeck, J. Phys. B: At. Mol. Opt. Phys. **16**, 1837 (1983).

64 G. Bieri, L. Asbrink, W. Von Niessen, J. Electron Spectrosc. Relat. Phenom. **27**, 129 (1982).

65 K. Kimura, S. Katsumata, T. Yamazaki, H. Wakabayashi, J. Electron Spectrosc. Relat. Phenom. **6**, 41 (1975).

66 V.S. Prabhudesai, V. Tadsare, S. Ghosh, K. Gope, D. Davis, and E. Krishnakumar, J. Chem. Phys. **141**, 164320 (2014).

67 S. I. Chu and A. Dalgarno, Phy. Rev. A **10**, 788 (1974).

68 N. T. Padial, D. W. Norcross, and L. A. Collins, J. Phys. B: At., Mol. Opt. Phys. **14**, 2901 (1981).

69 M. A. Morrison, Adv. At. Mol. Phys. **24**, 51 (1988).